Ocean Systems Engineering, *Vol. 7, No. 2 (2017) 157-177*
DOI: https:// doi.org/10.12989/ose.2017.7.2.157

Design and estimation of a sensing attitude algorithm for AUV self-rescue system

Yi-Ting Yang[a] and Sheng-Chih Shen[*]

Department of Systems and Naval Mechatronic Engineering, National Cheng Kung University, No.1, Daxue Rd., East Dist., Tainan City 701, Taiwan (R.O.C.)

(Received May 31, 2016, Revised May 8, 2017, Accepted May 10, 2017)

Abstract. This research is based on the concept of safety airbag to design a self-rescue system for the autonomous underwater vehicle (AUV) using micro inertial sensing module. To reduce the possibility of losing the underwater vehicle and the difficulty of searching and rescuing, when the AUV self-rescue system (ASRS) detects that the AUV is crashing or encountering a serious collision, it can pump carbon dioxide into the airbag immediately to make the vehicle surface. ASRS consists of 10-DOF sensing module, sensing attitude algorithm and air-pumping mechanism. The attitude sensing modules are a nine-axis micro-inertial sensor and a barometer. The sensing attitude algorithm is designed to estimate failure attitude of AUV properly using sensor calibration and extended Kalman filter (SCEKF), feature extraction and backpropagation network (BPN) classify. SCEKF is proposed to be used subsequently to calibrate and fuse the data from the micro-inertial sensors. Feature extraction and BPN training algorithms for classification are used to determine the activity malfunction of AUV. When the accident of AUV occurred, the ASRS will immediately be initiated; the airbag is soon filled, and the AUV will surface due to the buoyancy. In the future, ASRS will be developed successfully to solve the problems such as the high losing rate and the high difficulty of the rescuing mission of AUV.

Keywords: autonomous underwater vehicle; extended Kalman filtering; BPN classifier; AUV airbag

1. Introduction

Significant research is being conducted on the development of autonomy for underwater robotic vehicles, which are widely employed in many fields of application such as oceanographic, marine archaeology (Roman and Mather 2010), military organizations, off-shore oil industry, and cable tracking and inspection (Asakawa *et al*. 2002). The advent of underwater robotic vehicles has significantly reduced the dangers in deep sea exploration. Two kinds of robotic vehicles used in marine research are remotely operated vehicles (ROVs) and autonomous underwater vehicles (AUVs). The main difference between the two is that ROVs are connected to the ship by communication cables whereas AUVs operate independently from the ship. AUVs operate without an umbilical, therefore AUVs are able to conduct activities over a larger range. In our study, ASRS has the potential of predicting vehicular catastrophic and averting it, thereby minimizing loss of

∗Corresponding author, Professor, E-mail: scshen@mail.ncku.edu.tw
[a] Email: p16044031@mail.ncku.edu.tw

http://www.techno-press.org/?journal=ose&subpage=7 ISSN: 2093-6702 (Print), 2093-677X (Online)

the AUV.

In recent years, the micro-electro-mechanical systems(MEMS) has nearly become a vital technology for modern society because of its small volume, low power consumption, low cost and ease to integrate into systems or modify (Zhou and Mason 2002). MEMS technology creates entirely innovative kinds of products, such as gyroscope sensor in camera-shake detection systems (Hwangbo *et al.* 2013), multi-axis inertial motion sensors for smartphone-based navigation (Niu *et al.* 2012) and rehabilitation systems based on inertial measurement units (IMU) (Leardini *et al*. 2014). Additionally, the integration of Global Positioning System and inertial Navigation System (GPS/INS) is usually employed to measure the position of AUVs (Yun *et al*. 1999, Bonin-Font *et al.* 2015). Unfortunately, small errors in the measurement of initial data are double integrated into larger errors progressively in attitude data, and such errors increase unbounded. Error Reduction calibration for initialization of INS is paramount for the systematic parameter, like scale factor, bias and misalignment of axes. Based on the situation depicted above, a calibration method is investing and adopted in our study (Bao *et al*. 2013). There are many researches utilized Kalman filter (KF) (Luinge and Veltink 2005), complementary filter (CF) (Ruiz et al. 2012), adaptive Kalman filter (AKF) (Li and Wang 2013) or extended Kalman filter (EKF) (Mirzaei and Roumeliotis 2008) to fuse gyroscope and accelerometer together, taking advantages of their individual strength. One of the above, EKF is a form of non-linear estimation and typically used to compute the solution from these multiple sources. The EKF also developed by (Marins *et al*. 2001) allows estimating the orientation of attitude using IMUs. In this research, we chose the EKF to filter IMU outputs with a balance of noise cancelling and adaptability simultaneously, used in sensing attitude algorithm for ASRS.

However, the system is computationally complex due to values estimation of AUV, and causes the high dimension which is called “curse of dimensionality” which donates the drastic raise of computational complexity and the classification error (Aha *et al*. 1991). The purpose of feature extraction is to reduce the dimension of the large measurement datas and prevent program operation from out of memories. We adopted nine kinds of features to improve dimensionality reduction before send into the classifiers. Feature extraction is a technique for extracting a subset of new features from the original set by some functional ways which keep as much information in the data as possible (Biricik *et al.* 2012). Conventional Principal Component Analysis (PCA), which is orthogonal the eigenvectors of the covariance matrix, is one of the most widely used for feature extraction techniques and factor analysis (Wold *et al*. 1987). Hence, PCA was chosen to reduce the dimension of the AUV attitude value in this study. Feeding the value to the classifier to determine the conditions of AUV after feature extractions.

The sensing algorithm with EKF for sensing the attitude of AUV, while employing the backpropagation network (BPN) to classify motion data that are formed in the AUV. The neural network consists of multiple artificial neurons to receive inputs, and process them to obtain an output (Hopfield 1982). By repeating amendments to the model weights, neural network makes central processing unit (CPU) more logical to calculate the nonlinear systems of AUV motion (Sayyaadi and Ura 1999). Neural network has been widely used because of a number of advantages, including estimating which variables are important in classification, detecting possible interactions between predictor variables and constructing the prediction model with high accurate rate. Furthermore, neural network has emerged as an important tool in classification which has been investigated in many different important applications (Zhang 2000). In one work, Wenxi *et al.* (2005) designed a scalable mobile phone-based system for multiple vital signs monitoring and healthcare. Constructing neural network classifier (NNC) for classifying human activities by using

a wearable sensor. (Yang *et al.* 2008, Wang *et al.* 2012, Tuncel *et al.* 2009). As mentioned above, activity recognition is one of the most active application areas of NNC. In this research, NNC is used in the calculation of nonlinear systems AUV attitude data to detect a catastrophic failure of an AUV. We based on the multilayer feed-forward backpropagation algorithm as NNC and proposed an effective activity recognition method using 10-DOF sensor module. Backpropagation network (BPN) is the most widely used type of networks and is an efficient way to compute the gradient in a ANN (Rumelhart *et al.* 1986). This application is capable of reducing the probability of damaging and sinking the AUV.

The concept of ASRS comes from the vehicle safety device: airbags consists of a flexible fabric bag in order to protect occupant and restrict during a crash accident (Lund and Ferguson 1995, Burgess *et al.* 1995). Wang (2005) and Dragcevic *et al.* (2009) designed the airbags, which fires via a small pyrotechnic charge to increase motorcyclists safety protections while riding a motorcycle. The airbags are applied to not only fall-protection device but also automatic inflatable life by the inflatable method of gas cylinder (Guangyi *et al.* 2007, Toshiyo *et al.* 2008, Tamura *et al.* 2009, Ishizaka *et al.* 2014). We extended the airbags systems to load on the AUV with CO_2 cylinders to implement the ASRS. In this research, we developed a malformed detection algorithm for AUV with both SCEKF and ANN, and the Implementation of air bag system loaded on AUV is under way.

2. Theoretical methods and designs

This section presents an overview of the theoretical method on the formulation of sensors algorithm and classification. The former includes the sensors calibration and extended Kalman filter algorithm; the latter is constructed of feature extraction and neural classifier. Moreover, we designs the concept of the airbag system for ASRS. Fig. 1 shows an overview of the SARS scheme.

2.1 Sensors algorithm

The implemental detail of using IMU in the AUV will be explained in this section. It includes constructing the 10-DOF sensors module, sensors calibration and EKF algorithm.

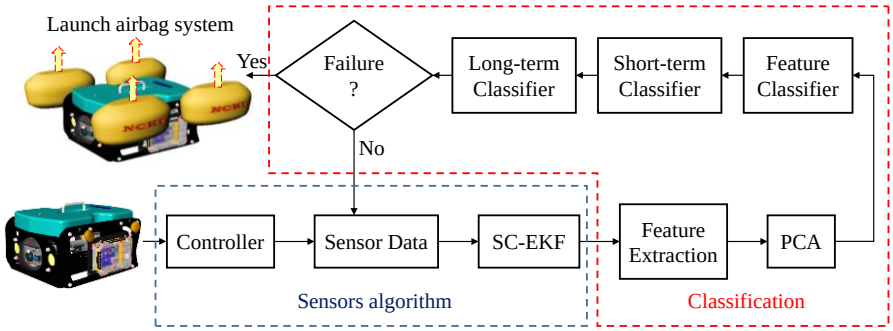

Fig. 1 An overview of the SARS scheme

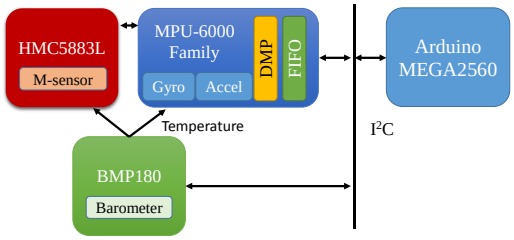

Fig. 2 Block diagram of the 10-DOF sensor module

2.1.1 Senor design

The MEMS sensor system contained 9-DOF IMU (three accelerometers, three gyroscopes, three magnetometers) and barometer integrated with microcontroller (Arduino MEGA2560). The six-axis inertial sensors (MPU6050) which is a complete triple axis gyroscope and triple axis accelerometer inertial sensing system are the most suitable sensors for stabilization and attitude measurement, where accelerometers track and eliminate the gyroscopes drift in vertical attitude (roll, pitch) of AUVs. The advantage of MPU6050 is that it eliminates the inter-axial differential problem between gyroscope and accelerometer and saves more space. MPU6050 contains the digital motion processor (DMP) which performs the motion processing algorithm itself. However, the horizontal attitude (yaw) is not possibility measurement. We used magnetometer (HMC5883L) with fusion algorithm accordingly for eliminating the gyroscope offset to recognize the AUV activity context more reliably. The barometer (BMP180) is used in ASRS to detect the depth of the AUV position and control the pressure of the air bag for supplying the perfect buoyancy. In addition, BMP180 also includes temperature sensor which is not only measure the underwater temperature but for thermal compensation for the MPU6050. The block diagram of the 10-DOF module as shown in Fig. 2.

2.1.2 10-DOF sensors data calibration

Although the development of the MEMS technology has made a great progress, the IMUs are difficult to be implemented a precision data in the presence of various errors, which categorizes into the deterministic error and the stochastic error (Titterton *et al.* 1997). Owing to the integration of IMU, any residual error will be accumulated and grow without bound, resulting in attitude data and orientation errors. That is the reason why the first step in using IMU is to calibrate its sensors. Calibration is the process of the measurement outputs comparing with known reference data and determining the coefficients that drive the output to agree with the reference data over a range of output. We can establish the error model illustrated in Fig. 3.

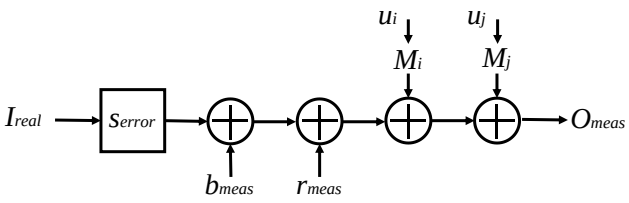

Fig. 3 The sensor error model

Where I_{real} is the real raw value of the input, O_{meas} represents the measurement of the output, scale factors s_{error}, biases b_{meas}, stochastic noise r_{meas} and M_i and M_j are the axial coupling factor corresponding with the u_i and u_j respectively. The relationship between sensor error model can be expressed using the following equation

$$O_{meas} = (1 + s_{error}) I_{real} + b_{meas} + M_i u_i + M_j u_j + r_{meas} \tag{1}$$

If further simplify the equation, the calibration errors during assembly of each component generated into the IMU module can be ignored. Therefore, the characteristic equation can be expressed as

$$O_{meas} = (1 + s_{error}) I_{real} + b_{meas} + r_{meas} \tag{2}$$

The position and velocity drift depends of scale factor, bias, and stochastic sensor error. Then it is very important the accurate procedure of calibration for an initialization of the IMU to improve the working efficiency the sensing element.

Stochastic noise: thermal noise

There is no temperature compensation when designing the IMU module, these variable type sensors are sensitive to temperature changes. The purpose of thermal compensation is to determine the adjustment in performance of a system when operated under different temperatures and to measure the desired variable precisely. There are two main approaches for thermal compensation: the thermal soak method and the thermal ramp method (Aggarwal *et al*. 2008). In this research, the thermal soak method was adopted to investigate thermal effect of IMU because of recording the sensor data until the element temperature stabilized. A method of linear interpolation has been used to establish the thermal compensation

$$\delta_r^T \times (T_2 - T_1) = \delta_r^{T2} (T - T_1) - \delta_r^{T1} (T + T_2) \tag{3}$$

where δ_r^{T1} and δ_r^{T2} are known at temperatures T_1 and T_1, T is the required temperature point and δ_r^T is a calculated IMU value at T℃. The thermal testing procedures of this research is to maintain constant temperature by utilizing the thermal turntable cabinet shown in Fig. 4. The variation of the thermal errors of IMU sensor is evaluated at temperatures ranging from 25℃ to 60℃.

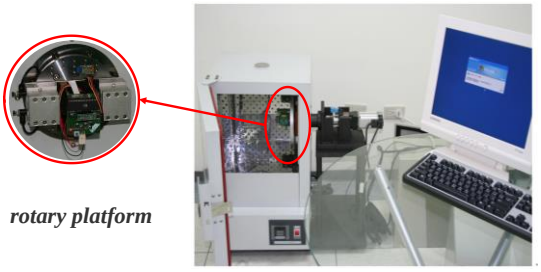

Fig. 4 Thermal turntable cabinet setup

Bias

First of all, conducting static output measurement to calculate the amount of the bias, and the static noise output should be low and be the well distributed stable signal within ideally condition. In order to minimize the error caused by bias, we averaged the IMU data to calculate the bias, which is deducted from the output values of IMU measurements. The Calculation formula of the bias value is by Eq. (4)

$$\mu = \frac{\sum_{i=1}^{n} \delta_{ri}}{n} \tag{4}$$

Where μ is the bias of IMU, δ_{ri} is the output values of IMU measurements and n represents the total number of samples.

Scale factor

The Linear relationship between input and output is one of a very important characteristic for an ideal inertial sensing element. Scale factor drifts of inertial sensors describe how well the relation between input and output IMUs are usually modeled with a linear response to simplify the calculation of measurement. we found the linear equation belongs to each components by linear least square (LLS) formula.

In order to find the coefficient of IMU linear equation, the scale factor is denoted as α_1, the offset coefficient is α_0, the corresponding value set in the user interface is $\delta_s = [\omega_s \; a_s \; m_s]^T$; $\delta_r = [\omega_r \; a_r \; m_r]^T$ is the real raw measurement data, where acceleration a, angular velocity ω, magnetic values m. The model function is given by Eq. (5)

$$\delta_s = \alpha_0 + \alpha_1 \delta_r \tag{5}$$

Using the following function was written it in matrix to find the coefficient of IMU linear equation

$$\min_{\alpha_1,\alpha_2} \left\| \begin{pmatrix} 1 & \delta_{r1} \\ \vdots & \vdots \\ 1 & \delta_{rn} \end{pmatrix} \begin{pmatrix} \alpha_0 \\ \alpha_1 \end{pmatrix} - \begin{pmatrix} \delta_{s1} \\ \vdots \\ \delta_{sn} \end{pmatrix} \right\|_2 \tag{6}$$

Then, the solution of parameter α_1 may then be simplified as

$$\alpha_1 = \frac{\sum_{i=1}^{n} \delta_{ri}\delta_{si} - n \cdot \bar{\delta}_r \bar{\delta}_s}{\sum_{i=1}^{n} (\delta_{ri})^2 - n \cdot (\bar{\delta}_r)^2} \tag{7}$$

where δ_{ri} and δ_{si} are the real raw and sample value at the i[th] orientation and rotation, respectively of all N samples. can be calculated as Eq. (8) by Eq. (5).

$$\alpha_0 = \bar{\delta}_s - \alpha_1 \bar{\delta}_r \tag{8}$$

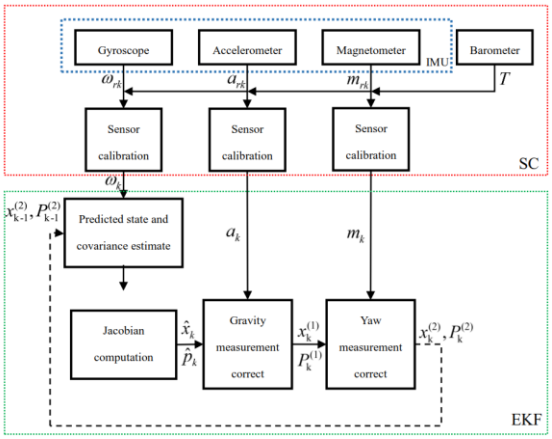

Fig. 5 Overview of the SCEKF structure

2.2 EKF algorithm

A quaternion based EKF is proposed in this section for determining the attitude of the AUV from the outputs of IMU. Attitude estimation is a very important part of the ASRS systems. If the initial data are double integrated into larger errors without bound, it brings on the misclassification of ANN algorithm with wrong attitude values. For the sake of this error, We used a series of measurements observed over time for signal processing. The main advantage of the KF is its ability to provide the quality of the estimate, whereas the KF only applies to the linear and Gaussian models. The EKF conversely is a form of non-linear version of the KF which linearizes about an estimate of the current mean and covariance (Sabatini 2006). In view of this, we chose the EKF to filter IMU outputs with a balance of noise cancelling and adaptability simultaneously, used in sensing attitude algorithm for ASRS. We proposed the EKF fusing with the accelerometer, gyroscope and magnetometer integrated with sensor calibration (SC). SCEKF results to an improvement of the orientation accuracy from IMU. A flow-chart of structure performed by the proposed SCEKF is capsuled in Fig. 5.

- Sensor calibration (SC)

The IMU calibration equation presented in Eqs. (3)-(5) and discussed in section 2.1.

- Compute the predict phase

$$\hat{x}_k = \Phi(T_s, \hat{\omega}_{k-1}) x_{k-1}^{(2)} + \hat{v}_{k-1} \tag{9}$$

$$\hat{P}_k = F_{k-1} P_{k-1}^{(2)} F_{k-1}{}^T + B_{k-1} Q B_{k-1}^T \tag{10}$$

First step of EKF predicts a current state and covariance matrix at time k. We estimated a current state based on the previous states $\hat{x}_{k-1} = \left[\hat{a}_{k-1}\ \hat{\omega}_{k-1}\ \hat{m}_{k-1}\right]^T$ which is composed of the gyroscope measurement $\hat{\omega}_{k-1}$ and white noise $\hat{v}_{k-1} = \left[{}^a\hat{v}_{k-1}\ {}^\omega\hat{v}_{k-1}\ {}^m\hat{v}_{k-1}\right]^T$ and the priori covariance matrix $\hat{P}_k$ based on a previous covariance matrix $P_{k-1}^{(2)}$, covariance Q and B_{k-1} is a state noise coefficient matrix.

- Jacobian computation

$$F_{k-1} = \frac{\partial \Phi}{\partial x}\Big|_{T_s, \hat{\omega}_{k-1}} = J_f(T_s, \hat{\omega}_{k-1}) \tag{11}$$

$$\tilde{y}_k = z_k - h(\hat{x}_k, 0), \quad H_k = \frac{\partial h}{\partial x}\Big|_{\hat{x}_k} = J_h(\hat{x}_k) \tag{12}$$

However, in view of the non-linear process of state transition F_{k-1} and observation H_k directly , EKF approach requires being estimated by computing the Jacobian.

- Gravity measurement correct

$$S_k = H_k \hat{P}_k H_k^T + R_a \tag{13}$$

$$K_k = \hat{P}_k H_k^T \left(H_k \hat{P}_k H_k^T + R_a\right)^{-1} \tag{14}$$

$$x_k^{(1)} = \hat{x}_k + K_k\left(a_k - H_k \hat{x}_k\right) \tag{15}$$

$$P_k^{(1)} = \left(I_{4\times 4} - K_k H_k\right)\hat{P}_k \tag{16}$$

Where the innovation covariance S_k based on a priori error covariance matrix $\hat{P}_k$ and the measurement covariance matrix of accelerometer R_a, which main diagonal elements are from the accelerometer values, non-main diagonal elements are all zero conversely. The Kalman gain K_k is the error covariance matrix after gravity measurement correct.

- Yaw measurement correct

$$S_k = H_k P_k^{(1)} H_k^T + R_m \tag{17}$$

$$K_k = P_k^{(1)} H_k^T \left(H_k P_k^{(1)} H_k^T + R_m\right)^{-1} \tag{18}$$

$$x_k^{(2)} = x_k^{(1)} + K_k\left(m_k - H_k x_k^{(1)}\right) \tag{19}$$

$$P_k^{(2)} = \left(I_{4\times 4} - S_k H_k\right)P_k^{(1)} \tag{20}$$

Where the measurement covariance matrix of magnetometers R_m, which main diagonal elements are from the magnetometer values, non-main diagonal elements are all zero conversely. $P_k^{(2)}$ is the error covariance matrix after yaw measurement corrected.

2.3 Structure of NNC

We are going to introduce the structure of NCC for recognition of AUV activties in this section. The NNC scheme is classified into two categories: the feature extraction and BPN algorithm which comprises a feature classifier, a short-term classifier, and a long-term classifier as shown in

Fig. 6. A sliding window technique cut the sensors data into 20 second in each short-term window with 50% overlapping.

In the beginning, for the purpose of reducing the dimension of the extracted features from the sensor data, these extracted features are selected by the PCA and feeding into the feature classifier to make a distinction of the AUV motions. Upon completion of the feature classifier construction, we are capable to distinguish every AUV motion in each operating period. This way is helpful for recognition the complex AUV activities and detecting each kind of motions well.

2.3.1 Feature extraction and selection

AUV motions are defined by the six degrees of freedom including heave, surge, sway, pitch, roll and yaw, and they are coupling by the vehicle shape, trends and current interaction. Therefore, the attitude data of AUV is the high dimension and very complex. The purpose of feature extraction is to reduce the dimension of the large measurement datas and prevent program operation from out of memories. The characteristics of a data segment is to keep the most meaning ful features and remove the redundant of data. Therefore, the feature extraction methods have been applied for activity detection from accelerometer data. (Saeedi and El-Sheimy 2015, Preece *et al*. 2009). İn order to extract feature easily, the continuous measurement data of sensors is divided into many overlapping segments of which each is 20 seconds time, was illustrated in Fig. 6. In this paper, we adopted the principal components analysis (PCA) as the feature selection procedure to lower the dimension of the original features (Krzanowski 1979). Feature extraction is highly subjective in nature, it depends on applications. Here, we introduced the following features that is beneficial to classification of AUV failure detection; used these features to discriminate the type of AUV activity (Ranganathan *et al*. 2001).

- Min,Max: minimum and maximum of the sensors signal.
- Mean: the mean value is computed over a window of sensors signal. In the below equation that W describes the number of elements of y

$$\bar{y} = \frac{\sum_{i=1}^{W} y_{\mathrm{i}}}{W} \tag{21}$$

- Interquartile range (IQR): The interquartile range of a segment can be calculated by integrating while the mean values of different classes are similar and compare of the spread of data in a data set.
- Root mean square (RMS): quadratic mean value of the signal

$$RMS = \sqrt{\frac{1}{W}\sum_{i=1}^{|W|} y_i^{\,2}} \tag{22}$$

- Standard deviation (STD): mean deviation of the sensors signal compared to the averge

$$STD = \sqrt{\frac{1}{W}\sum_{i=1}^{W} (y_i - \bar{y})^2} \tag{23}$$

- Root Mean Square Error (RMSE): the RMSE makes an general purpose deviation metric for each signal of sensor and is given by

$$RMSE = \frac{1}{W-1}\sum_{i=j}^{W}(y_j - \bar{y})^2 \tag{24}$$

- Signal magnitude area (SMA) (Bouten *et al.* 1997): SMA is the average of absolute acceleration over a window length and suitable for distinguishing between static and dynamic.

$$SMA: \frac{1}{W}\left(\sum_{i=1}^{W}\left|a_i^{sur}\right| + \sum_{i=1}^{W}\left|a_i^{swa}\right| + \sum_{i=1}^{W}\left|a_i^{hea}\right|\right), \tag{25}$$

where $a_i^{sur}, a_i^{swa}, a_i^{hea}$ represent ith of the acceleration of the surge, sway and heave respectively.

- Signal vector magnitude (SVM) (Karantonis *et al.* 2006): SVM distinguishes between shorter periods of activity and rest than SMA. It is able to detect the AUV is being attacked or hit the obstacles.

$$SVM: \sqrt{a_i^{sur^2} + a_i^{swa^2} + a_i^{hea^2}} \tag{26}$$

- Averaged acceleration energy (AEE): the AEE is the mean value of the energy over three acceleration to describes how the energy of sensors signal is. İt can validate for distinguish static activities. from dynamic activities.

2.3.2 BPN construction

Finally, these extracted features selected by the PCA are feeding into the feature classifier, short-term classifier and long-term classifier sequentially and output the AUV condition. In order to detect the AUV condition accurately, reliably, stably and robustly, we divided recognition system into three classifiers which are based on BPN. BPN is considered the workhorse of ANNs and is the multilayer perceptron (MLP) based on a feed forward algorithm. (Rumelhart *et al*. 1986). The hidden layers, between input and output layers, use the error back-propagation (BP) algorithm to compute nonlinear relationship in supervised learning. The main features of BPN are as follows: high learning accuracy, fast response and can process the nonlinear problems.

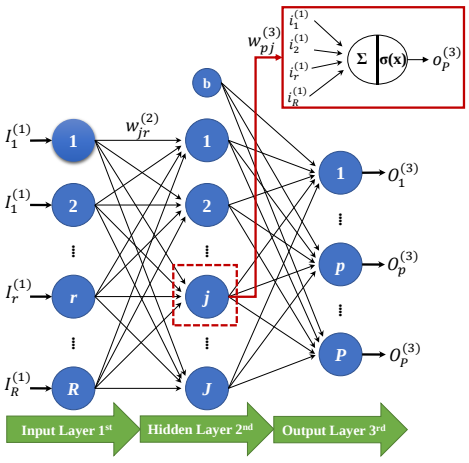

Fig. 7 The topology of the BPN classifier

In this paper, a three-layer BPN is used for classifying AUV failure condition. The topology of the BPN classifier as shown in Fig. 7 (Nielsen 2015). The input layer has R neurons, equal to the dimension of the feature vectors $I=\left[I_1^{(1)}, I_{\mathrm{r}}^{(1)},\ldots,I_{\mathrm{R}}^{(1)}\right]^T$, where superscript 1 indicates the 1st layer. The hidden layer has J neurons, and the output layer has P neurons, equal to the number of AUV condition $O=\left[O_1^{(3)}, O_{\mathrm{p}}^{(3)},\ldots,O_{\mathrm{P}}^{(3)}\right]^T$, where superscript 3 indicates the 3rd layer. $w_{pj}^{(3)}$ $w_{jr}^{(2)}$ denotes the weight from the hidden to the output layer and from the input to the hidden layer, respectively. $b^{(3)}, b^{(2)}$ denotes the bias in 3rd and 2nd layer respectively. The $i^{(\mathrm{n})}$ and $o^{(\mathrm{n})}$ is the input value and the activation of a neuron in the nth layer $\{n\in N: n\le 3\}$. We take the interval between hidden layer (2nd) and output layer (3rd) as an example. The function of the neurons in each step are defined as follows: (Rumelhart *et al.* 1986)

- In the BPN network, the intermediate quantity $net_j^{(3)}$ is the weighted input to the neurons in the 3rd layer, and implements a nonlinear transformation from the output values of the 2nd layer to the output values of the 3rd. σ is called the sigmoid function in general non-linear and differentiable. the functions of the pth neuron are given by

$$o_p^{(3)}=\sigma(net_j^{(3)})=\sigma(\sum_{j=1}^{J} w_{pj}^{(3)} o_j^{(2)}+b_p^{(3)}) \tag{27}$$

- The discrepancy $E^{(3)}$ between the desired output $t_p^{(3)}$ and the real output $O_p^{(3)}$ in 3rd layer can motivate the BP learning algorithm as gradient descent on sum-squared discrepancy. The factor of $1/2$ will simplify the exponent when differentiating later. The function is defined as

$$\mathrm{E}^{(3)}=\frac{1}{2}\sum_{p}(t_p^{(3)}-O_p^{(3)})^2 \tag{28}$$

- Then, adjusting the weights to find the partial derivative E with respect to a weight $w_{\mathrm{pj}}^{(3)}$: $\Delta w_{\mathrm{pj}}^{(3)}\propto -\eta(\partial E^{(3)}/\partial w_{\mathrm{pj}}^{(3)})$, However, the discrepancy is not directly the function of weights. Calculating the derivative of the discrepancy is done using the chain rule twice.

$$\Delta w_{pj}^{(3)}=-\eta\frac{\partial E^{(3)}}{\partial o_p^{(3)}}\frac{\partial o_p^{(3)}}{\partial net_p^{(3)}}\frac{\partial net_p^{(3)}}{\partial w_{pj}^{(3)}} \tag{29}$$

Let's discuss each of partial derivatives in turn:

- In the last term of Eq. (29) is the derivative of the net $net_p^{(3)}$ with respect to a weight $w_{pj}^{(3)}$:

$$\frac{\partial net_p^{(3)}}{\partial w_{pj}^{(3)}}=\frac{\partial}{\partial w_{pj}^{(3)}}(\sum_{j=1}^{J} w_{pj}^{(3)} o_j^{(2)}+b_p^{(3)})=o_j^{(2)} \tag{30}$$

- Next, the derivative of the activation $o_p^{(3)}$ with respect to the net input $net_p^{(3)}$:

$$\begin{aligned}\frac{\partial o_p^{(3)}}{\partial net_p^{(3)}} &= \frac{\partial}{\partial net_p^{(3)}}\sigma(net_p^{(3)}) \\ &= \sigma(net_p^{(3)})(1-\sigma(net_p^{(3)})) = o_p^{(3)}(1-o_p^{(3)})\end{aligned} \tag{31}$$

- Last, we consider the derivative of the E with respect to the activation. As a consequence of the neuron is in the output layer, then $O_p^{(3)}$ is equal to $o_p^{(3)}$.

$$\frac{\partial E}{\partial o_{\mathrm{p}}^{(3)}} = \frac{\partial E}{\partial \mathrm{O}_{\mathrm{p}}^{(3)}} = \frac{\partial(1/2(\mathrm{t}_{\mathrm{p}}^{(3)} - \mathrm{O}_{\mathrm{p}}^{(3)})^2)}{\partial \mathrm{O}_{\mathrm{p}}^{(3)}} = -(\mathrm{t}_{\mathrm{p}}^{(3)} - \mathrm{o}_{\mathrm{p}}^{(3)}) \tag{32}$$

- Finally, substituting these results Eqs. (30)-(32) back into original Eq. (29) to find the weight change $\Delta w_{pj}^{(3)}$ rule.

$$\Delta w_{pj}^{(3)} = \eta\overbrace{(\mathrm{t}_{\mathrm{p}}^{(3)} - \mathrm{o}_{\mathrm{p}}^{(3)})\mathrm{o}_{\mathrm{p}}^{(3)}(1-\mathrm{o}_{\mathrm{p}}^{(3)})}^{\varepsilon_p}\mathrm{o}_{\mathrm{j}}^{(3)} = \eta\varepsilon_p\mathrm{o}_{\mathrm{j}}^{(3)} \tag{33}$$

- We can find the weight change $\Delta w_{jr}^{(2)}$ in the same processes of above and is defined as:

$$\Delta w_{jr}^{(2)} = \eta\overbrace{\sum_{j}^{J}\varepsilon_p \mathrm{w}_{\mathrm{pj}}^{(3)}\mathrm{o}_{\mathrm{j}}^{(2)}(1-\mathrm{o}_{\mathrm{j}}^{(2)})}^{\varepsilon_j}\mathrm{o}_{\mathrm{r}}^{(1)} = \eta\varepsilon_j\mathrm{o}_{\mathrm{r}}^{(1)} \tag{34}$$

BPN algorithm approach to recognize and intelligent detect failures based on changes in weights values $\Delta w_{pj}^{(3)}$ $\Delta w_{jr}^{(2)}$ of the AUV feature parameters.

2.4 The concept of the airbag system

In the case of AUV failure and sinking underwater, we designed an airbag system to increase buoyancy and reduce the overall density of AUV. The AUV is 36 centimeter in length (14.2 inches), 20 centimeter Beam (7.9 inches), 2.8 kilograms while full load (6.2 pounds), 3.1 kilograms after putting the counterweight (6.8 pounds), and 3 knots (1.54 m/s). The vision is that we install a waterproof container system on both sides of AUV. The waterproof cabin, which length 20 cm, diameter 10 cm, 1570L of the displacement, including sensing module, double-trigger inflator, and airbag. Fig. 8(a) illustrates a double-trigger inflator includes a servo motor, horn, spring, spring case, striker, water soluble PVA fiber, and CO2 cylinder. The designed double-trigger inflator not only can trigger by electricity but also trigger by water damage when the waterproof cabin is severely broken.

There are two ways to trigger the inflator. To begin with the electricity trigger way, in the case of the waterproof cabin is watertight, after detecting the failure of AUVs, servo motor rotates for pushing the striker, and the striker punches the release button. CO2 releases into the air bag through the air tube as shown in Fig. 8(b).

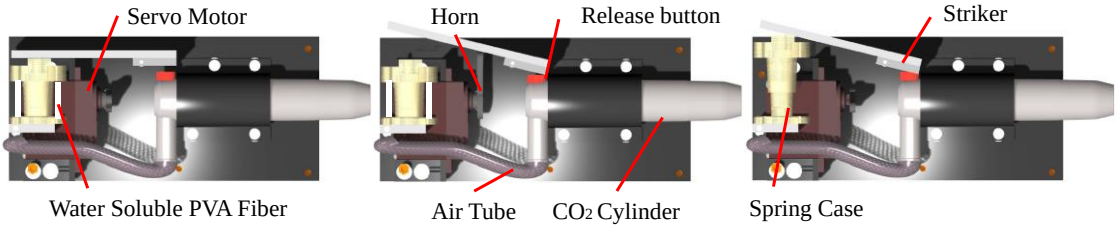

(a) Before release (b) release by servo motor (c) release by spring

Fig. 8 The design diagram of inflator

We chose MG995 for servo-motor which weights 55 grams; MG995 is sufficient to move the horn from the striker with it's maximum torque 13 kg-cm. Besides, if the AUV is severely impacted and cause the cabin seepage, so that the power system is damaged. The AUV can not resurface by the thruster or the electricity-trigger inflator. So we designed the water-trigger inflator for this kind of case. When the cabin is seeped, water melts the water soluble PVA fiber and release the spring case as shown in Fig. 8(c). The music wire is selected to spring within the spring case, the true maximum load of selected spring is 27.985N which have enough force to press the release button through striker.

In addition, if the total weight of a waterproof container and its substance is 1.25 kg; the total displacement and weight of an AUV are 3.61 kg and 4.36 kg respectively. Suppose that the acceleration of gravity is the constant 9.8 m / s^2. In other words, the total buoyancy of entire AUV apparatus is 32.73 Newton upwards contrary to the total gravitation is 42.63 Newton downwards. In the development of ASRS, we used two bottles of the12 g CO_2 gas cylinder with 6 L of CO_2 in, and four natural rubber inflatable nylon airbag with a capacity of 2.4L. The airbags connect with the regulating valves and cling to the valves to avoid falling and cause the pollution under the sea. Assume that the maximum depth is 100 m which refers to 11atm pressure there, and suppose that the temperature is regarded as Kelvin temperature 297K. According to the Ideal Gas law Eq. (35), where R is gas constant 8314.32 (N·m)/(kmol·K), n_{CO2} is 0.273, $V_{cylinder}$ is 0.014L of a 12 g canister, the pressure in a CO2 cylinder is 475atm, which is much higher than the water pressure 11atm. So the CO2 cylinder can operate successfully without body deformation. The relationship between flow rate and pressure is the following Eq. (36): (Guangyi *et al.* 2007)

$$\frac{n_{co2}RT}{V_{cylinder}} = P_{cylinder} \tag{35}$$

$$W_{12} = \frac{A_{12}P_1}{\sqrt{T_1}}\left\{\frac{2\gamma}{R_g(\gamma-1)}\left[\left(\frac{P_2}{P_1}\right)^{2/\gamma} - \left(\frac{P_2}{P_1}\right)^{\gamma+1/\gamma}\right]\right\}^{1/2} \tag{36}$$

where γ =1.2 and CO_2 Gas constant R_g = 188.9J/Kg·K.

3. Experimental test and result.

3.1 SCEKF

To validate the sensor calibration and fusion method proposed in this paper, this section covers the results obtained from the 10-DOF sensor module with operating system of Windows 8.1, 2.20 GHz CPU, 8GB memory, and experiments are performed with the Arduino described in Section 2.1.1. The system was fixed on an anti-vibration table to minimize interference. The proposed SCEKF algorithm was used to estimate accelerometer and orientation with 27-Hz updating rate.

As the calculation process of sensor algorithm, we used the rotary platform with outputting the quantitative and stable signal to observe the relative signal output. The rotary platform as shown in Fig. 4. The first process is that fixing IMU at the center and along the rotation axis of the platform and fixing it by valves. After the installation, setting the required rate or angle of rotation as a reference data by the user interface; we measured the output corresponding to the reference data. The performance of the orientation before/after SCEKF algorithm are presented in Fig. 9(a)-9(c), respectively; produced reasonable output values within the expected ranges. It is seen that each component of Euler orientation (i.e., roll, pitch, and yaw) is within 0·1 degree after SCEKF processing in the static test.

3.2 AUVs attitude simulation and experiment

In order to construct a robust underwater vehicle fault attitude database, we simulated the underwater vehicle motion model with different situations in the water environment, which can provide the particular case of attitude data, such as the AUVs suffered a crash or propeller disabled. Moreover, we built the fault simulator GUI interface for a more convenient operation, in other words, the ASRS start with the fault simulator GUI interface, after inputting the required AUVs dimensions, hydrodynamic coefficients, buoyancy center and, inertia coefficients. Next, simulator calculates the different AUV motion data under different case through the Matlab^{TM} program as shown in Fig. 10. The above results from simulator will combine with the experimental data as the database for training and verification of BPN classifier. Last but not least, the real AUV motion signal is set as the testing dataset to ensure the establishment of the ASRS. The modular modeling equation of AUVs is selected from (Prestero 2001). The modeling method of Prestero's without considering the sea conditions of emission that can help us to generate the dynamic models of AUVs quickly and conveniently. The dynamics model and kinematics model of AUVs are established by analysis of the force working on AUVs moving underwater, based on the theorem of the momentum of the rotation around the buoyancy center and the theorem of the motion of mass center. The motion in 6-DOF of the AUVs is determined. And then, the attitude data of AUVs at any instant are determined.

Since we simulated the AUV motion in the underwater environment without considering the influence of currents and waves, so we did the wave maker experiment in NCKU Ship Model Towing Tank to observe the changes and effects on the AUV motion data in different wave height. By experimenting with simulation, we can be closer to the state of the real ocean environment. The experiment of the AUVs affected by wave maker in NCKU Ship Model Towing Tank is illustrated in Fig. 11.

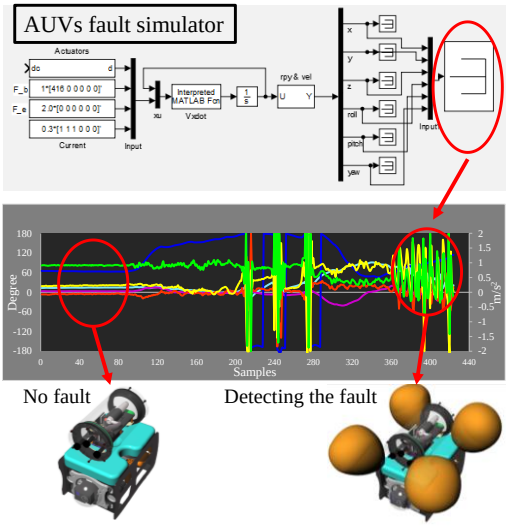

Fig. 10 The AUVs fault simulator diagram

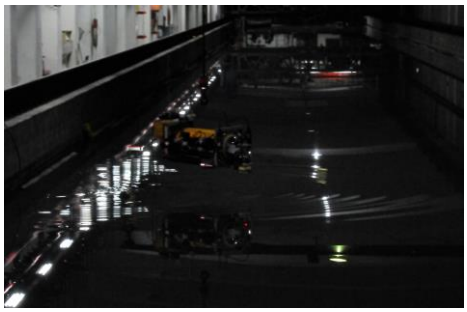

Fig. 11 The wave maker of the NCKU Ship Model Towing Tank

3.3 Classification results

In this paper, we focused on ten conditions of AUV which are listed in Table 1. There are two types of these AUV conditions. One of them is failure situation and the other is functional condition both which include five motion status of the AUV. We carried out twenty times of experiments for capturing data and verifying classifier. The data from 17 experiments was adopted in the training program of the recognition scheme; these data were obtained from the others experiments were used for testing the recognition performance. Note that, since the sampling frequency is 27.5 Hz, the total number of the short-term and long-term samplings for each activity of each experiment is 550 and 2200 respectively, which means 20 seconds per short-term window and 80 seconds per long-term window. The feature extraction of this paper based on 50% overlapping windows using 550 samples of window sizes to avoid information loss at the boundary of a single window. The dimension of a feature vector was 45 (an accelerometer × 3 axes × 9 features + a gyroscope × 3 axes × 6 feature). Fig12. illustrates the first 2200 data of accelerations and Euler orientations collected from the first experiment. The selected features of

sensors data enabled effective recognition of the conditions and were suggested for BPN training procedure. A computation program adopted the input features and activates the feature classifier learning procedure with the BP algorithm, and outputted the results to short-term classifier. Then, an AUV condition was distinguished by a long-term classifier which was inputted the several outcomes from short-term classifier to raise the accuracy of failure recognition. The number of neurons in each hidden layer are 4, 6, and 7 for the feature classifier, short-term classifier, and long-term classifier, respectively, and the number of epochs is 700 for each neural training, The BPN classifier was trained on the training data set and tested on the test set which are from the experiment values. The classifier was created by neural network toolbox of MATLAB^{TM} for practical implementation and to validate the proposed model.

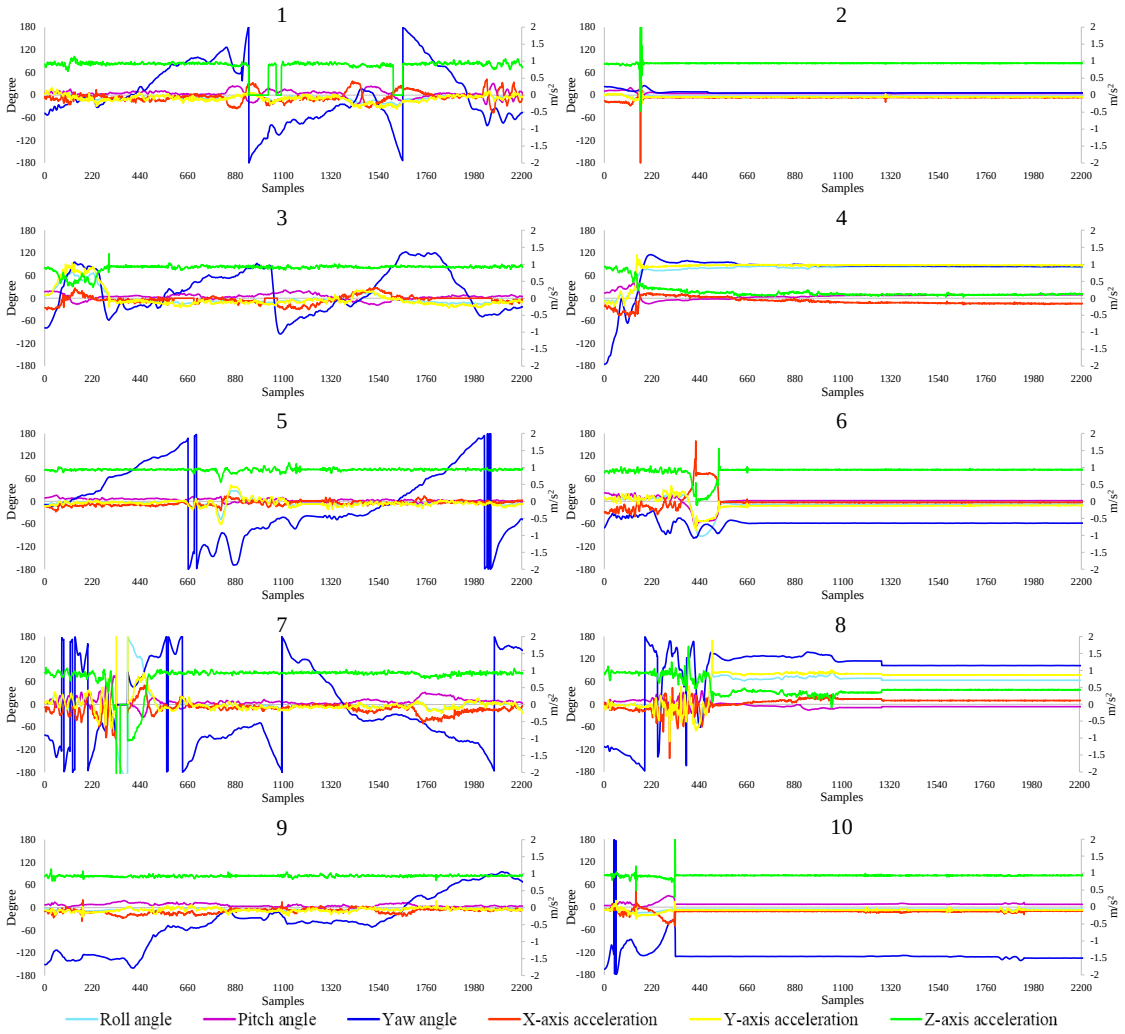

Fig. 12 The accelerations and Euler orientation of the first experiment

Table 1 Activities performed in this experiment

Number	Activity Description
1	Functional condition after horizontal sinking
2	Malfunction after horizontal sinking
3	Functional condition after vertical sinking
4	Malfunction after vertical sinking
5	Functional condition after ramped sinking
6	Malfunction after ramped sinking
7	Functional condition after turbulence
8	Malfunction after turbulence
9	Functional condition after collision
10	Malfunction after collision

Table 2 Confusion matrix for all the testing experiments

20 times of testing experiments													
Classified Type	1	2	3	4	5	6	7	8	9	10	Recognition Rate (%)	Detection Accuracy (%)	
1	14/13	0/0	1/2	0/0	5/6	0/0	0/0	0/0	0/0	0/1	70/65	Malfunction	97/92
2	1/2	16/14	0/0	0/0	0/0	1/2	0/0	0/1	2/3	2/4	80/70	Functional condition	93/88
3	1/1	0/0	15/13	0/0	0/1	0/0	0/0	0/0	1/1	0/0	75/65		
4	0/0	0/0	0/0	18/16	0/0	2/2	0/1	0/0	0/0	0/0	90/80		
5	4/3	0/0	2/4	0/1	15/13	0/0	0/0	0/0	0/1	0/0	75/65		
6	0/1	1/1	0/0	2/3	0/0	16/15	0/0	3/4	0/0	0/0	80/75		
7	0/0	0/0	0/0	0/0	0/0	0/0	17/15	1/2	0/0	0/0	85/75		
8	0/0	0/0	0/0	0/0	0/0	1/1	3/4	16/13	0/0	0/0	80/65		
9	0/0	1/2	2/1	0/0	0/2	0/0	0/0	0/0	16/14	1/2	80/70		
10	0/0	2/3	0/0	0/0	0/0	0/0	0/0	0/0	1/1	17/14	85/70		

*Proposed classifier with feature extraction in BP algorithm/ANN classifier without feature extraction

After building up our prediction algorithm, we apply our chosen prediction algorithm on our new test set which's from the real signal of AUV, in order to have an idea about the algorithm's performance on unseen data. The confusion matrix of all the real AUV testing experiments is provided in Table 2, which recorded the result from the 20 times experiment on each condition of AUV. We have implemented in two different ways under MATLAB^{TM} environment. In the first, we conducted in our proposed classifier system with feature extraction and the results indicate that the AUV failure detection on the average 97% of the time, and a successful functional condition accuracy of 93% is achieved. Second, we chose a classifier in ANN learning algorithm without feature extraction for comparing with the classifier that we proposed. The performance indicated that the ANN classifier without feature extraction performs poorer than our proposed. From the confusion matrix, we can know that the malfunction and functional condition are not easy to be confused. However, the motion within functional condition may be misclassified between each other, because these activities contains similar amplitude peak and waveform at the AUV.

3.4 Simulation and design of the inflator

Finally, we simulated the capacity change between the CO2 cylinder and the air bag to make sure it can be aerated successfully and save AUV to surface. In this research, the high-pressure CO2 gas cylinders were designed to install in the AUV, and detect the failure conditions by sensors module. The design specifications of inflator were explained in section 2.4, We adopted the BMP180 to measure the pressure where the AUV located. We simulated the time relation rate between depth and airbag volume changes determined by Eqs. (35) and *36). From the result of simulation illustrated in Fig. 13. It takes 32seconds to filled with four nylon airbags and provides 94.08N buoyancy for AUV. The design of added buoyancy can bring 13.45kgw of underwater vehicle to the surface (asume that the Full load displacement is fixed). The entire process takes about 50 seconds. Furthermore, we can install the appropriate number of gas cylinders and airbags in accordance with the different displacement of AUV. With this technology, we can install the appropriate number of gas cylinders and airbags in accordance with the different displacement of AUV.

4. Conclusions

The main objective of this work was to develop the intelligent AUV self-rescue system (ASRS) for detecting failure to minimize loss of an autonomous underwater vehicle (AUV). We combined three main ideas to construct the ASRS, including sensors algorithm, classifier conducting, and air bag system. Complex data acquisition was done by the 10-DOF sensors module with sensor calibration and extended Kalman filter (SCEKF), where Euler orientation fused with gravity and magnetic field are as state variables, can benefit to get the precise attitude from the AUV. After SCEKF processed, we extracted the features of these signals from the 10-DOF sensors module and selected these features by principal components analysis (PCA) method. The results were incorporated with feature classifier, short-term classifier, and long-term classifier in order to recognize 10 types of AUV condition. According to the experimental test in section 3, we have shown that the 20 experimental data sets are categorized into “malfunction” or “functional condition” categories. The outcomes of proposed classification with features extracted, which failure detection accuracy is 97%, were more accurate than the ANN without features extracted. These results confirmed that the technology of the ASRS was feasible and that the proposed methods were accurate. Furthermore, we designed an inflatable mechanism which fills CO_2 to the airbags to generate buoyancy for AUV while failure detection.

The attitude estimation and classification applied in the underwater environment is a new field.

Considering the future work,we will try to extend more condition types of AUV for classifying more complex situation and accomplish the airbag system for setting on the AUV. we can have the ability to construct a variety of different models for the AUVs fault simulation, such as the underwater turbulence or underwater creatures’ interference. To provide a more comprehensive ASRS, and do not have to do the experimental in the real underwater environ-ment, also can improve the performance and convenience of installation to the ASRS.With this technology, we can install the appropriate number of gas cylinders and airbags in accordance with the different displacement of AUV to avoid the loss of AUV; even can be used in rescuing vessels to reduce the shipwreck in the future, thereby minimizing loss of life and property. This study will have outstanding contributions for the next generation of underwater vehicles. We are look forward to

that the application of the SARS will be used widely in the future.

Acknowledgments

The authors would like to thank Ministry of Science and Technology (MOST) (granted number: MOST 103-2221-E-006-220-MY3, MOST 104-2622-E-006-019-CC2, MOST 105-2622-E-006-011-CC2, 105 AS-11.2.4-FA-F1 and 106 AS-18.1.7-FA-F1). The research was supported in part by the Headquarters of Advancement at the National Cheng Kung University, which is sponsored by the Ministry of Education, Taiwan.

References

Aggarwal, P., Syed, Z. and El-Sheimy, N. (2008), "Thermal calibration of low cost mems sensors for land vehicle navigation system", 2859-2863.

Aha, D.W., Kibler, D. and Albert, M.K. (1991), "Instance-based learning algorithms", *Machine Learning*, **6**(1), 37-66.

Asakawa, K., Kojima, J., Kato, Y., Matsumoto, S., Kato, N., Asai, T. and Iso, T. (2002), "Design concept and experimental results of the autonomous underwater vehicle AQUA EXPLORER 2 for the inspection of underwater cables", *Adv. Robot.*, **16**(1), 27-42.

Bao, Z., Lu, G., Wang, Y. and Tian, D. (2013), "A calibration method for misalignment angle of vehicle-mounted IMU", *Procedia - Social and Behavioral Sciences*, **96**, 1853-1860.

Biricik, G., Diri, B. and Sonmez, A.C. (2012), "Abstract feature extraction for text classification", *Turkish J. Elec. Eng. Comput. Sci.*, **20**, 1137-1159.

Bonin-Font, F., Massot-Campos, M., Lluis Negre-Carrasco, P., Oliver-Codina, G. and Beltran, J.P. (2015), "Inertial sensor self-calibration in a visually-aided navigation approach for a micro-AUV", *Sensors*, **15**(1), 1825-1860.

Bouten, C.V.C., Koekkoek, K.T.M., Verduin, M., Kodde, R. and Janssen, J.D. (1997), "A triaxial accelerometer and portable data processing unit for the assessment of daily physical activity", *IEEE T. Bio.- Med. Eng.*, **44**(3), 136-147.

Burgess, A.R., Dischinger, P.C., Oquinn, T.D. and Schmidhauser, C.B. (1995), "Lower-extremity injuries in drivers of airbag-equipped automobiles - clinical and crash reconstruction correlations", *J. Trauma-Injury Infection Critical Care*, **38**(4), 509-516.

Dragcevic, Z., Takeuchi, K., Vecaj, D. and Hursa, A. (2009), "Motorcycle jacket with integrated air bag", *Tekstil*, **58**(7), 346-351.

Guangyi, S., Cheung-Shing, C., Guanglie, Z., Li, W.J., Leong, P.H.W. and Leung, K.S. (2007), "Towards a mobile airbag system using MEMS sensors and embedded intelligence", 634-639.

Hopfield, J.J. (1982), "Neural networks and physical systems with emergent collective computational abilities", *Proceedings of the National Academy of Sciences of the United States of America-Biological Sciences*, **79**(8), 2554-2558.

Hwangbo, M., Kim, J.S. and Kanade, T. (2013), "IMU self-calibration using factorization", *IEEE T. Robot.*, **29**(2), 493-507.

Ishizaka, S., Moromugi, S., Kobayashi, M., Kajihara, H., Koga, K., Sugahara, H., Ishimatsu, T., Kurata, S., Kirkness, J.P., Oi, K. and Ayuse, T. (2014), "A remote-controlled airbag device can improve upper airway collapsibility by producing head elevation with jaw closure in normal subjects under propofol anesthesia", *IEEE J. Translational Eng. Health Med.*, **2**, 1-9.

Karantonis, D.M., Narayanan, M.R., Mathie, M., Lovell, N.H. and Celler, B.G. (2006), "Implementation of a real-time human movement classifier using a triaxial accelerometer for ambulatory monitoring", *IEEE T. Inform. Technol. Biomed.*, **10**(1), 156-167.

Krzanowski, W.J. (1979), "Between-groups comparison of principal components", *J. Am. Statist. Association*, **74**(367), 703-707.

Leardini, A., Lullini, G., Giannini, S., Berti, L., Ortolani, M. and Caravaggi, P. (2014), "Validation of the angular measurements of a new inertial-measurement-unit based rehabilitation system: comparison with state-of-the-art gait analysis", *J. Neuroeng. Rehabilit.*, **11**, 7.

Li, W. and Wang, J.L. (2013), "Effective adaptive Kalman filter for MEMS-IMU/magnetometers integrated attitude and heading reference systems", *J. Navigation*, **66**(1), 99-113.

Luinge, H.J. and Veltink, P.H. (2005), "Measuring orientation of human body segments using miniature gyroscopes and accelerometers", *Med. Biol. Eng. Comput.*, **43**(2), 273-282.

Lund, A.K. and Ferguson, S.A. (1995), "Driver fatalities in 1985-1993 cars with airbags", *J. Trauma-Injury Infection Critical Care*, **38**(4), 469-475.

Marins, J.L., Xiaoping, Y., Bachmann, E.R., McGhee, R.B. and Zyda, M.J. (2001), "An extended Kalman filter for quaternion-based orientation estimation using MARG sensors", 2003-2011 vol.2004.

Mirzaei, F.M. and Roumeliotis, S.I. (2008), "A Kalman filter-based algorithm for IMU-camera calibration: observability analysis and performance evaluation", *IEEE T. Robot.*, **24**(5), 1143-1156.

Nielsen, M.A. (2015), "*Neural networks and deep learning*", Determination Press, Canada

Niu, X., Zhang, Q., Li, Y., Cheng, Y. and Shi, C. (2012), "Using inertial sensors of iPhone 4 for car navigation", 555-561.

Preece, S.J., Goulermas, J.Y., Kenney, L.P.J. and Howard, D. (2009), "A comparison of feature extraction methods for the classification of dynamic activities from accelerometer data", *IEEE T. Bio.- Med. Eng.*, **56**(3), 871-879.

Prestero, T.T.J. (2001), *Verification of a six-degree of freedom simulation model for the REMUS autonomous underwater vehicle*, Massachusetts institute of technology.

Ranganathan, N., Patel, M.I. and Sathyamurthy, R. (2001), "An intelligent system for failure detection and control in an autonomous underwater vehicle", *IEEE T .Syst. Man Cy. A*, **31**(6), 762-767.

Roman, C. and Mather, R. (2010), "Autonomous underwater vehicles as tools for deep-submergence archaeology", *Proceedings of the Institution of Mechanical Engineers Part M-Journal of Engineering for the Maritime Environment*, **224**(4), 327-340.

Ruiz, A.R.J., Granja, F.S., Honorato, J.C.P. and Rosas, J.I.G. (2012), "Accurate pedestrian indoor navigation by tightly coupling foot-mounted IMU and RFID measurements", *IEEE T. Instrum. Meas.*, **61**(1), 178-189.

Rumelhart, D.E., Hinton, G.E. and Williams, R.J. (1986), "Parallel distributed processing: explorations in the microstructure of cognition, vol. 1", (Eds., David, E.R., James, L.M. and Group, C.P.R.), 318-362, MIT Press.

Sabatini, A.M. (2006), "Quaternion-based extended Kalman filter for determining orientation by inertial and magnetic sensing", *IEEE T. Bio.- Med. Eng.*, **53**(7), 1346-1356.

Saeedi, S. and El-Sheimy, N. (2015), "Activity recognition using fusion of low-cost sensors on a smartphone for mobile navigation application", *Micromachines*, **6**(8), 1100-1134.

Sayyaadi, H. and Ura, T. (1999), "Multi input-multi output system identification of AUV systems by neural network", 201-208.

Tamura, T., Yoshimura, T., Sekine, M., Uchida, M. and Tanaka, O. (2009), "A wearable airbag to prevent fall injuries", *IEEE T. Bio.- Med. Eng.*, **13**(6), 910-914.

Titterton, D.H., Weston, J.L. and Institution of Electrical, E. (1997), "Strapdown inertial navigation technology".

Toshiyo, T., Takumi, Y. and Masaki, S. (2008), "A study to demonstrate the use of an air bag device to prevent fall-related injuries", 1-3.

Tuncel, O., Altun, K. and Barshan, B. (2009), "Classifying human leg motions with uniaxial piezoelectric gyroscopes", *Sensors*, **9**(11), 8508-8546.

Wang, L. (2005), "Air bags for motorcycles", *Chem. Eng. News*, **83**(39), 80-80.
Wang, Z., Jiang, M., Hu, Y. and Li, H. (2012), "An incremental learning method based on probabilistic neural networks and adjustable fuzzy clustering for human activity recognition by using wearable sensors", *IEEE T. Inform. Technol. Biomed.*, **16**(4), 691-699.
Wenxi, C., Daming, W., Shuxue, D., Michael, C., Hui, W., Shigeru, T. and Naotoshi, T. (2005), "A scalable mobile phone-based system for multiple vital signs monitoring and healthcare", *Int. Pervas. Comput.*, **1**(2), 157-163.
Wold, S., Esbensen, K. and Geladi, P. (1987), "Principal component analysis", *Chemometr. Intell. Lab.*, **2**(1-3), 37-52.
Yang, J.Y., Wang, J.S. and Chen, Y.P. (2008), "Using acceleration measurements for activity recognition: An effective learning algorithm for constructing neural classifiers", *Pattern Recogn. Lett.*, **29**(16), 2213-2220.
Yun, X., Bachmann, E.R., McGhee, R.B., Whalen, R.H., Roberts, R.L., Knapp, R.G., Healey, A.J. and Zyda, M.J. (1999), "Testing and evaluation of an integrated GPS/INS system for small AUV navigation", *IEEE J. Oceanic Eng.*, **24**(3), 396-404.
Zhang, G.Q.P. (2000), "Neural networks for classification: A survey", *IEEE T. Syst. Man C*, **30**(4), 451-462.
Zhou, J.W. and Mason, A. (2002), "Communication buses and protocols for sensor networks", *Sensors*, **2**(7), 244-257.

MK